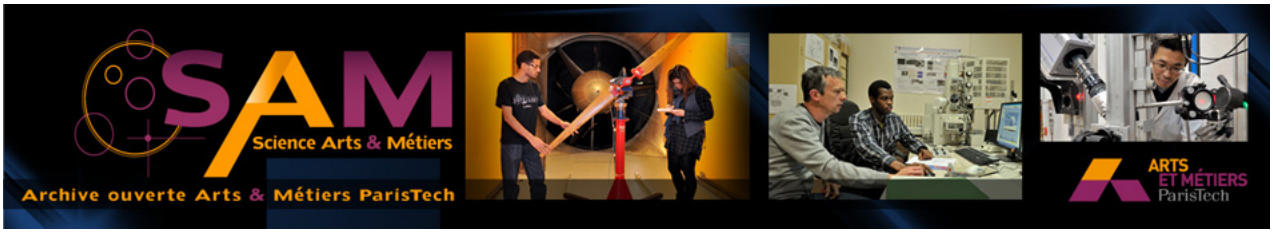

# Investigations on the mechanical properties of the elementary thin films composing a $CuIn_{1-x}Ga_xSe_2$ solar cell using the nanoindentation technique

Hocine Yacine Abib [a,b,*], Alain Iost [c], Alex Montagne [c], Khadidja Rahmoun [a], Boubakeur Ayachi [b], Jean-Pierre Vilcot [b]

[a] Material and Renewable Energies Research Unit URMER, University of Tlemcen Abou Bakr Belkaid, BP 119, Tlemcen 13000, Algeria
[b] Electronic, Microelectronics and Nanotechnology Institute IEMN, UMR 8520, - Avenue Poincare, - CS 60069 59652 Villeneuve d'Ascq cedex, France
[c] Mechanics, Surfaces and Materials Processing - MSMP, Arts et Métiers Paris Tech, — Lille Campus, 8, Boulevard Louis XIV, 59046 Lille, France

ARTICLE INFO

*Article history:*
Received 15 May 2016
Received in revised form 18 October 2016
Accepted 4 November 2016
Available online xxxx

*Keywords:*
Copper indium gallium selenide
Solar cells
Mechanical properties
Hardness
Young's modulus
Nanoindentation

ABSTRACT

In this investigation, the mechanical properties of the different layers composing a $CuIn_{1-x}Ga_xSe_2$ (CIGS) based solar cell were studied. Magnetron sputtering technique was used for the deposition of these layers except for the cadmium sulphide (CdS) layer which was deposited using chemical bath deposition process. We performed several indentation tests on the individual layers, i.e. molybdenum (Mo) back contact layer, CIGS absorber layer, CdS and alternative zinc sulphide oxide (ZnOS) buffer layers, and zinc oxide (ZnO)-AZO (aluminium-doped zinc oxide) transparent window layer; all were deposited on glass substrates. We report the values of the hardness ($H$) and of the Young's modulus ($E$) for each material, using indentation tests and an analytical model. The Mo layer remained the hardest and the most rigid, with $H = 8.7$ GPa and $E = 185$ GPa, while the CIGS layer has shown poor mechanical properties with $H = 3$ GPa and $E = 58$ GPa. On the other hand, the observed similarity in mechanical properties of the ZnO and ZnOS layers might be attributed to the similarity of their microstructures.


## 1. Introduction

$CuIn_{1-x}Ga_xSe_2$ (CIGS) based solar cell has been intensively investigated, but only a few works so far have reported on their mechanical properties [1,2]. The mechanical holding of the different layers composing a CIGS based solar cell is believed to highly affect the longevity of this cell. Therefore, studying fundamental mechanical properties of the different layers composing a CIGS solar cell is a real need. Nanoindentation is a well-known method for materials characterization and has a considerable interest in the field of thin films. Its principle lies in pressing a very small and hard tip of known geometry and mechanical properties, also called indenter, on the surface of the material to be characterized. The resulting imprint is used to deduce the mechanical properties of the investigated material. We used this method to determine the value for data of the hardness ($H$) and of Young's modulus ($E$) in the different elementary layers composing a CIGS based solar cell, i.e. molybdenum (Mo) back contact layer, CIGS absorber layer, cadmium sulphide (CdS) and alternative zinc sulphide oxide (ZnOS) buffer layers, and zinc oxide (ZnO) and aluminium-doped zinc oxide transparent (AZO) window layers.

The details of sample preparation technique and nanoindentation experiment are given in Section 2. Section 3 presents the Jönsson and Hogmark (JH) model [3] that has been used to interpret the raw experimental data and Section 4 gives the extracted values for hardness and Young's modulus for each layer.

## 2. Experimental procedure

### 2.1. Samples preparation

Prior to the deposition process, the 2-in. soda lime glass substrates (SLG) were chemically cleaned with acetone, ethanol and deionised water in an ultrasonic bath for 10 min, each step, and were then dried under $N_2$ flux, before being loaded into the sputtering machine (Alliance-Concept CT200). To prevent any contamination of the thin films caused by residual gas, the deposition chamber was initially pumped down to $2.93 \times 10^{-4}$ Pa. All sputtered thin films were deposited using an Ar flux of 10 sccm while deposition pressures were controlled using a butterfly valve. The 500 nm-thick Mo layer was deposited using the DC magnetron sputtering mode. The 2.5 μm-thick CIGS layer was pulsed DC-sputtered without an intentional heating from a single

* Corresponding author at: Electronic, Microelectronics and Nanotechnology Institute IEMN, UMR 8520, - Avenue Poincare, - CS 60069 59652 Villeneuve d'Ascq cedex, France.
*E-mail addresses:* hocine.abib@iemn.univ-lille1.fr (H.Y. Abib), alain.iost@ensam.eu (A. Iost), alex.montagne@ensam.eu (A. Montagne), k_rahmoun@mail.univ-tlemcen.dz (K. Rahmoun), boubakeur.ayachi@etudiant.univ-lille1.fr (B. Ayachi), jean-pierre.vilcot@iemn.univ-lille1.fr (J.-P. Vilcot).

quaternary CIGS target; after the film deposition, a recrystallization annealing process was carried at atmospheric pressure, under $N_2$ atmosphere at about 550 °C, using a rapid thermal annealing furnace (JetFirstJIPELEC 200). The 50 nm-thick CdS layer was deposited using a chemical bath deposition process, while the 60 nm-thick $ZnS_xO_{1-x}$layer was deposited at room temperature using co-sputtering from two targets: ZnO and ZnS. The50 nm and 300 nm-thick ZnO and AZO layers were RF-sputtered from ZnO target and 3% in weight$Al_2O_3$-doped ZnO target, respectively. The thickness of each layer was deduced from surface profilometry measurements (DektakXT stylus surface profiler). The deposited layers morphology and cross section were observed using field emission gun-scanning electron microscope (FEG-SEM, Zeiss Ultra 55). The crystalline structure of the layers was analysed with X-ray Diffraction (XRD) equipment (Rigaku SMARTLAB) in Bragg-Brentano mode with Cu-Kα radiation.

### 2.2. Nanoindentation experiment

Indentation tests were performed using an XP instrument (MTS, USA) equipped with a Berkovich diamond tip. A minimum of nine indents have been performed on each sample. The nanoindenter worked in strain-rate controlled mode, set at the constant value of 0.05 $s^{-1}$. Tests were performed using the CSM (Continuous Stiffness Measurement) mode [4], allowing a continuous characterization of H and E during the indentation process. The indenter reached a maximum penetration depth of at least the thickness of the film plus 300 nm in order to observe the influence of the substrate. Neighbouring indents were spaced by 35 times the maximal penetration depth, to avoid interactions. The calibration for the Berkovich indenter was performed by means of a fused silica standard. A constant value of the elastic modulus of approximately 72 GPa was obtained when reached above 10 nm of penetration depth, taking into account the surface effect and the indenter imperfections. Considering respectively the empirical 10% and the 1% rule of thumb for the indentation depth of coating for hardness and for modulus determination, it seemed difficult to get the correct values of some of the thin films elaborated in this study. For these materials, even for small indentation depths, the mechanical properties depend on the coating and on the substrate effect. For this reason we used a JH model [5], previously developed in order to determine these influences depending on the indented depth, from where the indentation with the greater indentation depth are an indication of the substrate mechanical properties.

## 3. Theory

The JH model [3] was used to calculate the film hardness when the indenter penetration is influenced by the substrate. The composite hardness $H_c$ that represents both the contribution of the film and of the substrate, is given by the area law of mixture:

$$H_c = \frac{A_f}{A}H_f + \frac{A_s}{A}H_s \quad (1)$$

With

$$\frac{A_f}{A} = \frac{2Ct_f}{h} - \frac{C^2{t_f}^2}{h^2} \quad (2)$$

where $h = h_f + h_s$ represents the total indentation depth; $A_f$ and $A_s$ respectively represents the film and substrate areas transmitting the mean contact pressure; $H_f$ the film hardness; $H_s$ the substrate hardness; $A = A_f + A_s$ is the total indented area, and $t_f$ the film thickness.

The geometrical constant, $C$, depends on the behaviour of the film material under indentation and also depends on the indenter geometry [3,6]. Employing a Berkovich indenter, $C = 0.0915$ if the film undergoes fracture under indentation loading, $C = 0.1746$ if the film undergoes plastic deformation, and $C = 1$ in a confined contact situation [5]. Fig. 1 represents the model when the film is plastically strained to match the shape of the Berkovich diamond tip.

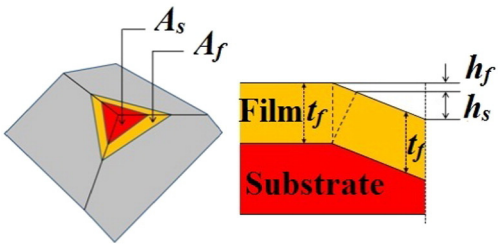


**Fig. 1.** Schematic representation the plastic deformation of a film coated on substrate. $h = h_f + h_s$ is the total indentation depth, $A_f$ and $A_s$ respectively the film and substrate area transmitting the mean contact pressure, $A = A_f + A_s$ the total indented area and $t_f$ the film thickness.

Combining Eq. (1) with Eq. (2) gives:

$$H_c = \left(2\frac{Ct_f}{h} - \frac{C^2{t_f}^2}{h^2}\right)H_f + \left(1 - 2\frac{Ct_f}{h} + \frac{C^2{t_f}^2}{h^2}\right)H_s \quad (3)$$

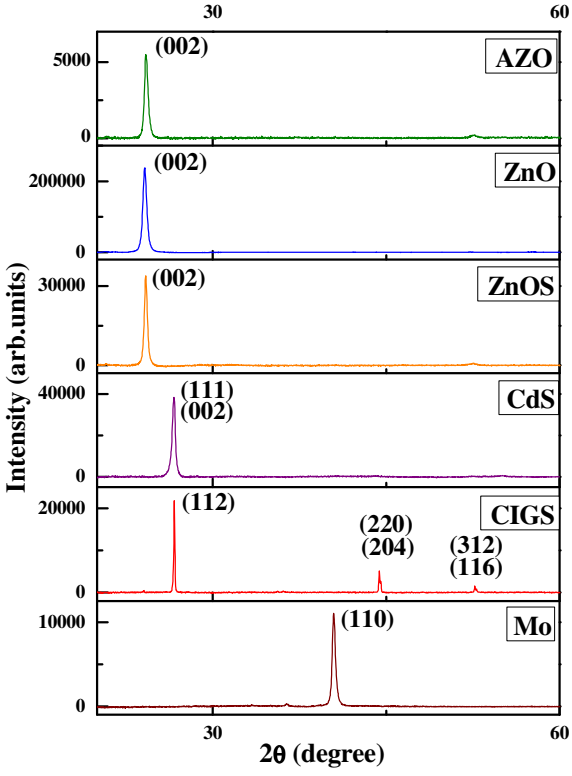


**Fig. 2.** XRD patterns of the layers (Mo, CIGS, CdS, ZnOS, ZnO and AZO).

**Table 1**
Crystallographic structure and preferred orientation of the layers (Mo, CIGS, CdS, ZnOS, ZnO and AZO).

| Layer material | Crystallographic structure | Preferred orientation |
|---|---|---|
| Mo | Cubic | (110) |
| CIGS | Chalcopyrite (tetragonal) | (112) |
| CdS | Cubic | (111) |
| | Wurtzite | (002) |
| ZnOS | Wurtzite | (002) |
| ZnO | Wurtzite | (002) |
| AZO | Wurtzite | (002) |

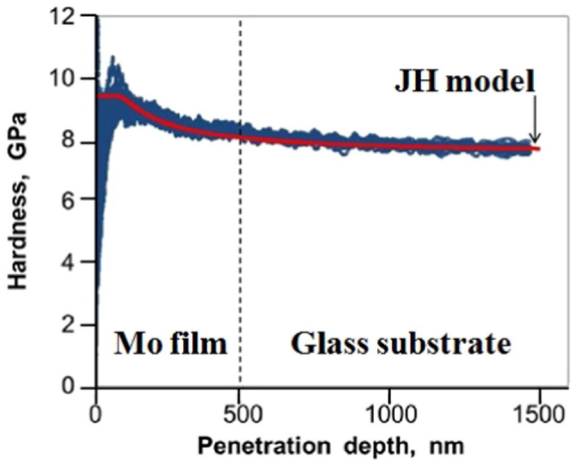


**Fig. 3.** Hardness variation versus the penetration depth for the 500 nm Mo film on SLG substrate. The solid line corresponds to the interpretation of the experimental results by the JH model.

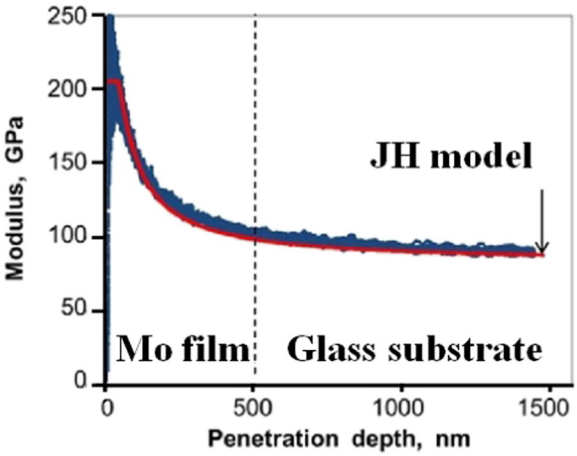


**Fig. 4.** Young's modulus variation with the penetration depth for the 500 nm Mo film on SLG substrate. The solid line corresponds to the interpretation of the experimental results by the JH model.

$A_s/A$ must be in the range of 0 to 1 [6,7]. For example, if the indentation depth is lower than the seventh of the film thickness, then $A_f = A$; $A_s = 0$ and therefore $H_c = H_f$. This model was generalised to multilayers materials [5,8,9].

The same model was used to determine the modulus of each layer, considering $C$ as a variable depending on the material. This constant was lower than the value used for the determination of the hardness, since the elastic zone extended further than the plastic zone.

## 4. Results and discussions

XRD analyses were performed in order to check out the crystalline structure and orientation, as well as the composed phases, of each thin film. All thin films were found to be a highly oriented single phase, as shown in Fig. 2. The observed preferred orientation was attributed to both the sputtering technique and to the plans energy. The crystallographic structure and orientation of each thin film are summarized in Table 1.

We used nanoindentation tests to determine the hardness and the Young's modulus of the SLG substrate, the glass has a reverse indentation size effect being attributed to cracking [10], afterwards the model was applied to extract the film's data values H and E.

The 500 nm Mo layer coated on SLG substrate is highly uniform and presents a columnar crystal structure, the Mo layer shows good mechanical properties, in agreement with the model for ductile behaviour, which can vary depending on the type of substrate and on the thickness of the layer [11,12]. Figs. 3 and 4 show respectively the evolution of the Mo's H and E with penetration depth, according to the model. The same procedure has been applied for each of the other layers and Table 2 shows the results H and E for all materials used in this study.

We observed a small pop-in on the CIGS force-displacement curve presented in Fig.5, for a load of 320 ± 20 mN and a displacement of 2100 ± 70 nm; other pop-ins are visible at 700 mN- –3000 nm, 1200 mN–3800 nm and 1600 mN–4300 nm. The CIGS coating with a compact morphology is either porous (Figs. 6b and 7b) or has a weak behaviour. CIGS's H and E increased with an increasing annealing temperature Table 2. During the early stage of penetration, the coating was confined between the indenter and the substrate and was compacted (work-hardening) until that the tip of the indenter came close to the substrate, H increased then to 4.45 GPa. From a penetration

**Table 2**
Value of the hardness and Young's modulus for the different materials. *H*: Hardness, *E*: Young's modulus.

| | | This work | | From literature | | | |
|---|---|---|---|---|---|---|---|
| Layer material | Thickness $t_f$ (nm) | $H_f$ (GPa) | $E_f$ (GPa) | $H_l$ (GPa) | $E_l$ (GPa) | (Substrate type, deposition technique, annealing temperature if any) | |
| SLG substrate | $10^6$ | 7.5 | 77 | 5.37 | 72 | (SLG) | [21] |
| | | | | 5.5–11.2 | / | (SLG) | [22] |
| Mo | 500 | 8.7 | 185 | 8.3–11.5 | 110–170 | (Polyimide, sputtering, 698 K) | [9] |
| | | | | 6–11 | 110–320 | (Titanium, sputtering) | [10] |
| CIGS | 2500 | 3–4.45 | 58 | | 29–75 | (Mo, co-evaporation) | [2] |
| | | | | 0.7–1.53 | 64.3–73.4 | (Polyimide, sputtering, 698 K) | [9] |
| | | | | 0.7–2.2 | 35–75 | (Glass, co-evaporation, 673–773 K) | [12] |
| | | | | | 70.4 ± 6.5 | (SLG, co-evaporation, 823 K) | [23] |
| | | | | | 68.9 ± 12.4 | (SLG, sputtering, 823 K) | [23] |
| CdS | 50 | 2.8 | 30 | 1.87–2.37 | 28.2–40.11 | (Glass, CBD,573 K) | [14] |
| ZnO | 50 | 5.5 | 100 | 4.95–7.8 | / | (Sapphire, epitaxy) | [16] |
| | | | | 8 | 110 | (Polyester, sputtering) | [17] |
| | | | | 9.2–7.2 | 168.6–139.5 | (Silicon, ALD, 573–773 K) | [18] |
| | | | | 5 ± 0.1 | 112 ± 4.7 | (Bulk ZnO single crystals) | [24] |
| | | | | 4–6 | 68–125 | (Silicon, sputtering) | [25] |
| ZnOS | 60 | 5.5 | 100 | / | / | | |
| AZO | 300 | 8.4 | 110 | | 29–75 | (Mo, co-evaporation) | [2] |
| | | | | 6.8–11.6 | 94.7–127.6 | (Glass, sputtering, 573–773 K) | [19] |
| | | | | 7.4–8.7 | 97.7–107 | (PET, sputtering) | [20] |
| | | | | 10.2 | 130 | (Glass, sputtering) | [26] |
| | | | | 1.76–5.11 | 28.7–628.9 | (ITO, sputtering) | [27] |

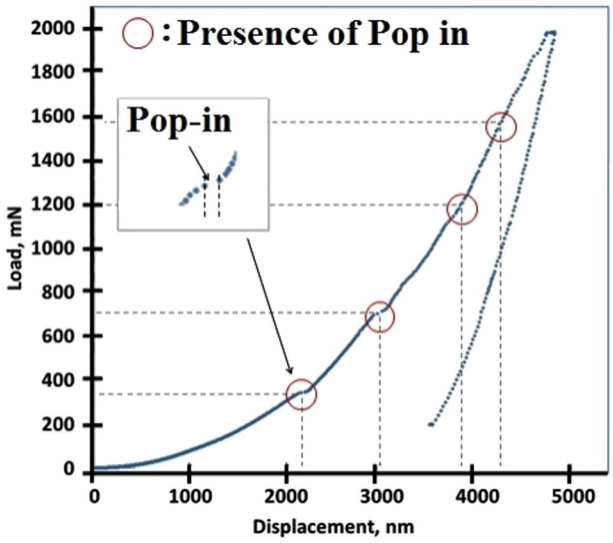


**Fig. 5.** A typical loading-unloading curve obtained for 2.5 μm CIGS layer deposited on SLG substrate. Pop-ins are visible at a load of 320 ± 20 mN and a displacement of 2100 ± 70 nm,700 mN–3000 nm, 1200 mN–3800 nm and 1600 mN–4300 nm.

depth of about 2300 nm, the substrate begins to interact and the measured resulting in an increase of the H value. This behaviour is similar to that observed for ductile coatings deposited on hard substrates [5, 13] for hardness and Young's modulus. Fig. 6 shows the layers surface morphology and Fig. 7 shows their cross-section. Simultaneously the loss of cohesion of the coating to the substrate appeared which was visible on the residual fingerprint and could be associated to pop-in for a load of 320 ± 20 mN and a displacement of 2100 ± 70 nm.

CdS film has an elasto-plastic behaviour and it was very difficult to distinguish its morphology from the cross-sectional view in Fig. 7c. Moreover, the annealing process could have strongly affected its

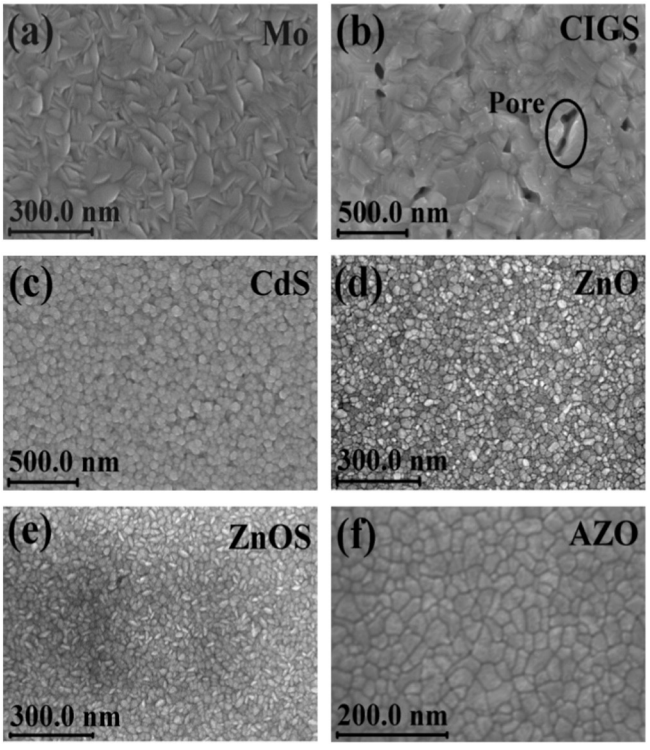


**Fig. 6.** SEM pictures of surface morphology for the different investigated materials: a) Mo, b) CIGS, c) CdS, d) ZnO, e) ZnOS and f) AZO.

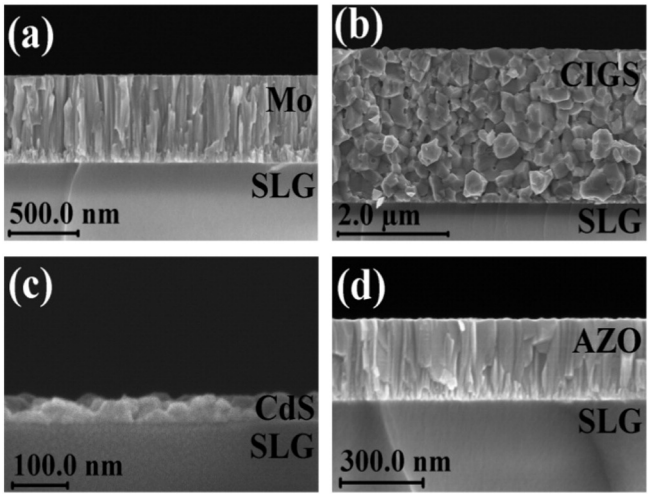


**Fig. 7.** SEM cross-sectional views of main layers: a) Mo, b) CIGS, c) CdS and d) AZO (similar views are obtained for all ZnO based materials and are not reproduced here).

crystallization, the surface morphology, and its microstructure, reducing the crystalline defects and the micro strains on the film [14] and would potentially improve its mechanical properties.

As predicted by Thornton's model [15], a low temperature sputtering deposition resulted in a columnar structure for the deposited material which is clearly seen on Fig. 7a, b and d. A similar morphology as well as an almost comparable composition of the ZnO and ZnOS layers explains the identical mechanical properties obtained. ZnO thin films deposited on polyester or sapphire substrates have the same mechanical properties, nevertheless ZnO layer's H and E decreased during the annealing process Table 2. AZO layer has presented almost the same hardness than the ZnO and the ZnOS layers, annealing increases hardness and Young's modulus of AZO thin film Table 2.

## 5. Conclusion

The JH model [3] was used to extract the hardness of the different elementary material layers constituting a CIGS solar cell. As expected, the Mo layer exhibited good mechanical properties, reinforcing its choice as a common back contact for thin film cells. The CIGS coating was either porous or had a weak behaviour. One might attribute the comparable mechanical properties of the ZnO, ZnOS and AZO layers to the similarity of their microstructures.

In a near future, tests of the mechanical properties of multilayer structure as well as of those of the entire cell will be performed in order to establish a multilayer model and to study the influence of the layers in relation to one another, and these ad hoc tools will be presented.

## Acknowledgements

This work was partly supported by the French RENATECH network.

## References

[1] T.H. Fang, Y.J. Hsiao, C.H. Lu, in: T.H. Meen, S. Prior, D. Kin-Tak Lam (Eds.), Innovation, Communication and Engineering, CRC Press, ISBN: 978-1-138-00117-6, 2014.
[2] T.H. Fang, Y.J. Hsiao, S.H. Kang, Mechanical characteristics of copper indium gallium diselenide compound nanopillars using in situ transmission electron microscopy compression, Scr. Mater. 108 (2015) 130–135.
[3] B. Jönsson, S. Hogmark, Hardness measurement of thin films, Thin Solid Films 114 (1984) 257–269.
[4] W.C. Oliver, G.M. Pharr, Measurement of hardness and elastic modulus by instrumented indentation, J. Mater. Res. 19 (2004) 3–20.
[5] K. Rahmoun, A. Iost, V. Keryvin, G. Guillemot, N.E. Chabane Sari, A multilayer model for describing hardness variations of aged porous silicon low-dielectric-constant thin films, Thin Solid Films 518 (2009) 213–221.

[6] A. Iost, R. Bigot, Hardness of coatings, Surf. Coat. Technol. 80 (1996) 117–120.
[7] G. Guillemot, A. Iost, D. Chicot, Comments on the paper "Modification of composite hardness models to incorporate indentation size effects in thin films", D. Beegan, S. Chowdhury, M.T. Laugier, Thin Solid Films 516 (2008) 3813–3817, Thin Solid Films 518 (2010) 2097–2101.
[8] E.S. Puchi-Cabrera, M.H. Staia, A. Iost, Modeling the composite hardness of multilayer coated systems, Thin Solid Films 578 (2015) 53–62.
[9] E.S. Puchi-Cabrera, M.H. Staia, A. Iost, A description of the composite elastic modulus of multilayer coated systems, Thin Solid Films 583 (2015) 177–193.
[10] H. Li, R.C. Bradt, The effect of indentation-induced cracking on the apparent micro hardness, J. Mater. Sci. 31 (1996) 1065–1070.
[11] Y.C. Lin, X.Y. Peng, L.C. Wang, Y.L. Lin, C.H. Wu, S.C. Liang, Residual stress in CIGS thin film solar cells on polyimide, J. Mater. Sci. Mater. Electron. 25 (2014) 461–465.
[12] S.M. Deambrosis, E. Miorin, F. Montagner, V. Zin, M. Fabrizio, M. Sebastiani, F. Massimi, E. Bemporad, Structural, morphological and mechanical characterization of Mo sputtered coatings, Surf. Coat. Technol. 266 (2015) 14–21.
[13] B. Arrazat, V. Mandrillon, K. Inal, Nanoindentation de couches dures ultra minces de ruthénium sur Or, Mater. Tech. 99 (2011) 245–252.
[14] E. Yücel, O. Şahin, Effect of pH on the structural, optical and nanomechanical properties of CdS thin films grown by chemical bath deposition, Ceram. Int. 42 (2016) 6399–6407.
[15] J.A. Thornton, Influence of apparatus geometry and deposition conditions on the structure and topography of thick sputtered coatings, Vac. Sci. Technol. 11 (1974) 666.
[16] V.A. Coleman, J.E. Bradby, C. Jagadish, Mechanical properties of ZnO epitaxial layers grown on a- and c-axis sapphire, Appl. Phys. Lett. 86 (2005) 203105s.
[17] K.A. Sierros, D.A. Banerjee, N.J. Morris, D.R. Cairns, I. Kortidis, G. Kiriakidis, Mechanical properties of ZnO thin films deposited on polyester substrates used in flexible device applications, Thin Solid Films 519 (2010) 325–330.
[18] C.Y. Yen, S.R. Jian, G.J. Chen, C.M. Lin, H.Y. Lee, W.C. Ke, Y.Y. Liao, P.F. Yang, C.T. Wang, Y.S. Lai, J.S.C. Jang, J.Y. Juang, Influence of annealing temperature on the structural, optical and mechanical properties of ALD-derived ZnO thin films, Appl. Surf. Sci. 257 (2011) 7900–7905.
[19] S.R. Jian, Y.Y. Lin, W.C. Ke, Effects of thermal annealing on the structural, electrical and mechanical properties of Al-doped ZnO thin films deposited by radio-frequency magnetron sputtering, Sci. Adv. Mater. 5 (2013) 7–13.
[20] R.C. Chang, T.C. Li, C.W. Lin, Influence of various thickness metallic interlayer's on opto-electric and mechanical properties of AZO thin films on PET substrates, Appl. Surf. Sci. 258 (2012) 3732–3737.
[21] N. Bouaouadja, M. Madjoubi, M. Kolli, C. Bousbaa, M. Hamidouche, Etude des possibilités d'amélioration de la transmission optique d'un verre sodocalcique érodé par sablage, Verres Céramiques et Composites 1 (2011) 43–51.
[22] C.R. Kurkjian, G.W. Kammlott, M.M. Chaudhri, Indentation behavior of soda-lime silica glass, fused silica and single-crystal quartz at liquid nitrogen temperature, J. Am. Ceram. Soc. 78 (1995) 737–744.
[23] S. Luo, J.H. Lee, C.W. Liu, J.M. Shieh, C.H. Shen, T.T. Wu, D. Jang, J.R. Greer, Strength, stiffness, and microstructure of Cu(In,Ga)Se2 thin films deposited via sputtering and co-evaporation, Appl. Phys. Lett. 105 (2014) 011907.
[24] S.O. Kucheyev, J.E. Bradby, J.S. Williams, C. Jagadish, Mechanical deformation of single-crystal ZnO, Appl. Phys. Lett. 80 (2002) 956–958.
[25] T.H. Fang, W.J. Chang, C.M. Lin, Nanoindentation characterization of ZnO thin films, Mater. Sci. Eng. A-452–453 (2007) 715–720.
[26] Z. Yun, W. Yue, W.P. Fei, L.H. Yu, W.S. Yu, Optical and mechanical properties of transparent conductive Al-doped ZnO films deposited by the sputtering method, Chin. Phys. Lett. 29 (2012) 038103.
[27] T.H. Fang, S.H. Kang, Surface and physical characteristics of ZnO:Al nanostructured films, J. Appl. Phys. 105 (2009) 113512.